AFRL-VA-WP-TP-2004-301

RECONFIGURABLE CONTROL DESIGN FOR THE X-40A WITH IN-FLIGHT SIMULATION RESULTS

Michael W. Oppenheimer and David B. Doman

FEBRUARY 2004

Approved for public release; distribution is unlimited.

AIR VEHICLES DIRECTORATE
AIR FORCE RESEARCH LABORATORY
AIR FORCE MATERIEL COMMAND
WRIGHT-PATTERSON AIR FORCE BASE, OH 45433-7542

REPORT DOCUMENTATION PAGE

Form Approved
OMB No. 0704-0188

1. REPORT DATE *(DD-MM-YY)*	2. REPORT TYPE	3. DATES COVERED *(From - To)*
February 2004	Conference Paper Preprint	

4. TITLE AND SUBTITLE
RECONFIGURABLE CONTROL DESIGN FOR THE X-40A WITH IN-FLIGHT SIMULATION RESULTS

5a. CONTRACT NUMBER
In-house

5b. GRANT NUMBER

5c. PROGRAM ELEMENT NUMBER
N/A

6. AUTHOR(S)
Michael W. Oppenheimer and David B. Doman

5d. PROJECT NUMBER
N/A

5e. TASK NUMBER
N/A

5f. WORK UNIT NUMBER
N/A

7. PERFORMING ORGANIZATION NAME(S) AND ADDRESS(ES)
Control Theory Optimization Branch (AFRL/VACA)
Control Sciences Division
Air Vehicles Directorate
Air Force Research Laboratory, Air Force Materiel Command
Wright-Patterson AFB, OH 45433-7542

8. PERFORMING ORGANIZATION REPORT NUMBER
AFRL-VA-WP-TP-2004-301

9. SPONSORING/MONITORING AGENCY NAME(S) AND ADDRESS(ES)
Air Vehicles Directorate
Air Force Research Laboratory
Air Force Materiel Command
Wright-Patterson Air Force Base, OH 45433-7542

10. SPONSORING/MONITORING AGENCY ACRONYM(S)
AFRL/VACA

11. SPONSORING/MONITORING AGENCY REPORT NUMBER(S)
AFRL-VA-WP-TP-2004-301

12. DISTRIBUTION/AVAILABILITY STATEMENT
Approved for public release; distribution is unlimited.

13. SUPPLEMENTARY NOTES
Conference paper to be presented at the AIAA Guidance, Navigation, and Control Conference, Providence, RI, 16-19 August 2004. This material is declared a work of the U.S. Government and is not subject to copyright protection in the United States.

14. ABSTRACT

In order to increase survivability and maximize performance, autonomous vehicles require the development of algorithms that fulfill the role of an adaptive human pilot in response to failures, damage, or uncertain vehicle dynamics. Hence, the guidance and control algorithms implemented on autonomous vehicles must be able to react and compensate, whenever possible, for failures so that their impact can be minimized. In this work, an adaptive reconfigurable inner-loop controller is developed for a modified version of the X-40A Space Maneuvering Vehicle. The purpose of this inner-loop control system is to accurately track body-frame angular velocity vector commands, while automatically reacting to and compensating for failures, damage, or uncertain vehicle dynamics.

15. SUBJECT TERMS
Reconfigurable control, dynamic inversion, in-flight simulation

16. SECURITY CLASSIFICATION OF:			17. LIMITATION OF ABSTRACT:	18. NUMBER OF PAGES	19a. NAME OF RESPONSIBLE PERSON (Monitor)
a. REPORT	b. ABSTRACT	c. THIS PAGE			Michael W. Oppenheimer
Unclassified	Unclassified	Unclassified	SAR	16	19b. TELEPHONE NUMBER *(Include Area Code)* (937) 255-8490

Reconfigurable Control Design For The X-40A With In-Flight Simulation Results

Michael W. Oppenheimer *
David B. Doman †
Air Force Research Laboratory, WPAFB, OH 45433-7531

1 ABSTRACT

In order to increase survivability and maximize performance, autonomous vehicles require the development of algorithms that fulfill the role of an adaptive human pilot in response to failures, damage, or uncertain vehicle dynamics. Hence, the guidance and control algorithms implemented on autonomous vehicles must be able to react and compensate, whenever possible, for failures so that their impact can be minimized. In this work, an adaptive reconfigurable inner-loop controller is developed for a modified version of the X-40A Space Maneuvering Vehicle. The purpose of this inner-loop control system is to accurately track body-frame angular velocity vector commands, while automatically reacting to and compensating for failures, damage, or uncertain vehicle dynamics. The combination of an inner-loop reconfigurable control law with an adaptive guidance loop and trajectory reshaping algorithm forms an integrated adaptive guidance and control algorithm. In-flight simulation results of the reconfigurable controller, guidance adaptation logic, and trajectory reshaping algorithm are shown for a simulated X-40A. The General Dynamics Total In-Flight Simulator research aircraft was used to generate the results. The flight test results shown here focus on reconfigurable control by investigating the inner-loop behavior for two different failure modes.

2 INTRODUCTION

The goal of dynamic inversion in flight control design is to cancel the wing-body forces and moments with control effector forces and moments such that the vehicle can accurately track body-axis rate commands generated by a guidance and control interface. The reconfigurable control law developed here is based on dynamic inversion with explicit model following coupled with an optimization based control allocator. The dynamic inversion control law[1] requires the use of a control effector allocation algorithm, because the number of control effectors on the X-40A exceeds the number of controlled variables and actuator rate and position limits must be enforced. The modified X-40A used in this project has 6 control surfaces, namely, left and right rudder-vators, left and right flaperons, speedbrake, and bodyflap. The speedbrake and bodyflap appear on the X-40A's larger cousin, the X-37, however they are not present on the original X-40A. Because there are 6 control sur-

*Electronics Engineer, 2210 Eighth Street, Bldg. 146, Rm. 305, Ph. 937-255-8490, Email Michael.Oppenheimer@wpafb.af.mil

†Senior Aerospace Engineer, 2210 Eighth Street, Bldg. 146, Rm. 305, Ph. 937-255-8451, Email David.Doman@wpafb.af.mil

faces and only 3 axes to control, it is possible that the desired control variable rate commands can be achieved in many different ways and so the control allocation algorithm is used to provide a unique solution to such problems.[2,3] To complete the inner-loop, prefilter blocks are designed to produce the desired closed-loop dynamics. In this work, an explicit model-following prefilter scheme is introduced so the inner-loop bandwidth can be adjusted by modifying the bandwidth of the explicit model when all control power is exhausted in one or more axes. When this situation occurs, known as axis saturation, the inner-loop bandwidth is reduced in order to reduce the demands on the actuators and this information (bandwidth) is passed to the adaptive guidance loop.[4] The adaptive guidance loop, in turn, modifies its gains when inner-loop saturation occurs to reduce the demands on the inner-loop. When the inner-loop becomes unsaturated, the bandwidth is increased back to its nominal value.

In this paper, details of the development of the inner-loop reconfigurable control law for the X-40A are provided. Section 3 discusses the dynamic inversion controller, Section 4 describes the control allocation algorithm, while the prefilters are developed in Section 5. In-flight simulation results are provided in Section 6, while conclusions are presented in Section 7.

3 DYNAMIC INVERSION

A dynamic inversion control law is developed for a modified version of the X-40A Reusable Launch Vehicle. The original X-40A utilized four aerodynamic control surfaces, namely, two flaperons and two rudddervators. Unfortunately, this number of control effectors limits the reconfiguration capabilities of the vehicle. In order to provide more redundancy, a speedbrake and a bodyflap were added to the aerodynamic model. The modified X-40A, with six control effectors, provides a wide range of recoverable failures.

An outer-loop adaptive guidance system generates body-frame angular velocity commands (p_{des}, q_{des}, r_{des}), that the inner-loop control system attempts to track. The dynamics of the body-frame angular velocity vector for a lifting body can be written as

$$\dot{\boldsymbol{\omega}} = \mathbf{f}(\boldsymbol{\omega}, \mathbf{P}) + \mathbf{g}(\mathbf{P}, \boldsymbol{\delta}) \qquad (1)$$

where $\boldsymbol{\omega} = [\mathrm{p\ q\ r}]^T$, p, q, and r are the rolling, pitching, and yawing rates, respectively, $\mathbf{P}$ denotes measurable or estimable quantities that influence the body-frame states, and $\boldsymbol{\delta} = (\delta_1, \delta_2, \cdots, \delta_n)^T$ is a vector of control surface deflections. The vector $\mathbf{P}$ contains variables such as angle of attack, sideslip, Mach number, and vehicle mass properties. The term $\mathbf{g}(\mathbf{P}, \boldsymbol{\delta})$ includes the control dependent accelerations, while the term $\mathbf{f}(\boldsymbol{\omega}, \mathbf{P})$ describes accelerations that are due to the base-vehicle's (wing-body) aerodynamic properties. It is assumed that the mass properties of the X-40A are constant, thus, the time derivative of the inertia matrix can be set to zero, i.e., $\dot{\mathbf{I}} = \mathbf{0}$. Then, Equation 1 can be written as[5]

$$\dot{\boldsymbol{\omega}} = \mathbf{I}^{-1}(\mathbf{G}_B(\boldsymbol{\omega}, \mathbf{P}, \boldsymbol{\delta}) - \boldsymbol{\omega} \times \mathbf{I}\boldsymbol{\omega}) \qquad (2)$$

where

$$\begin{aligned} \mathbf{G}_B(\boldsymbol{\omega}, \mathbf{P}, \boldsymbol{\delta}) &= \mathbf{G}_{WB}(\boldsymbol{\omega}, \mathbf{P}) + \mathbf{G}_\delta(\mathbf{P}, \boldsymbol{\delta}) \\ &= \begin{bmatrix} L \\ M \\ N \end{bmatrix}_{WB}^T + \begin{bmatrix} L \\ M \\ N \end{bmatrix}_\delta^T \end{aligned} \qquad (3)$$

In Equations 2 and 3, $\mathbf{I}$ is the inertia matrix and L, M, and N are the rolling, pitching, and yawing moments. In Equation 3, $\mathbf{G}_{WB}(\boldsymbol{\omega}, \mathbf{P})$ is the moment generated by the base aerodynamic system (wing-body system) and $\mathbf{G}_\delta(\mathbf{P}, \boldsymbol{\delta})$ is the total moment vec-

tor produced by the control effectors. Therefore,

$$\begin{aligned} \mathbf{f}(\omega, \mathbf{P}) &= \mathbf{I}^{-1}[\mathbf{G}_{WB}(\omega, \mathbf{P}) - \omega \times \mathbf{I}\omega] \\ \mathbf{g}(\mathbf{P}, \delta) &= \mathbf{I}^{-1}\mathbf{G}_{\delta}(\mathbf{P}, \delta) \end{aligned} \quad (4)$$

In order to utilize a linear control allocator, it is necessary that the control dependent portion of the model be linear in the controls. Hence, an affine approximation is developed such that

$$\mathbf{G}_{\delta}(\mathbf{P}, \delta) \approx \widetilde{\mathbf{G}}_{\delta}(\mathbf{P})\delta + \epsilon(\mathbf{P}, \delta) \quad (5)$$

The term $\epsilon(\mathbf{P}, \delta)$ is an intercept term[6] for the body-axis angular accelerations which is used to improve the accuracy of linear control allocation algorithms. Using Equations 1, 4, and 5, the model used for the design of the dynamic inversion control law becomes

$$\dot{\omega} = \mathbf{f}(\omega, \mathbf{P}) + \mathbf{I}^{-1}\widetilde{\mathbf{G}}_{\delta}(\mathbf{P})\delta + \mathbf{I}^{-1}\epsilon(\mathbf{P}, \delta) \quad (6)$$

The objective is to find a control law, that provides direct control over $\dot{\omega}$, so that $\dot{\omega} = \dot{\omega}_{des}$. Hence, the inverse control law must satisfy

$$\dot{\omega}_{des} - \mathbf{f}(\omega, \mathbf{P}) - \mathbf{I}^{-1}\epsilon(\mathbf{P}, \delta) = \mathbf{I}^{-1}\widetilde{\mathbf{G}}_{\delta}(\mathbf{P})\delta \quad (7)$$

Equation 7 provides the dynamic inversion control law that is used to set up a control allocation problem.

4 CONTROL ALLOCATION

Since there are more control effectors (6) than controlled variables (3) and the control effectors are restricted by position and rate limits, a control allocation algorithm is necessary. For the X-40A, there are three controlled variables, namely, roll, pitch, and yaw accelerations, while there are six control surfaces. Hence, a control allocation scheme must be used to insure that Equation 7 is satisfied. The control allocation scheme uses the mixed optimization linear programming technique of Bodson.[3]

To begin development of the allocator, let the left-hand side of Equation 7 be defined as $\mathbf{d}_{des}$ and denote the right-hand side of Equation 7 as $\mathbf{B}\delta$. Here, $\mathbf{d}_{des}$ are the body-axis accelerations that must be produced by the control effectors and $\mathbf{B}$ is the control effectiveness matrix defined as

$$\mathbf{B} = \mathbf{I}^{-1}\widetilde{\mathbf{G}}_{\delta}(\mathbf{P}) = \mathbf{I}^{-1}\begin{bmatrix} \frac{\partial L}{\partial \delta_1} & \frac{\partial L}{\partial \delta_2} & \cdots & \frac{\partial L}{\partial \delta_n} \\ \frac{\partial M}{\partial \delta_1} & \frac{\partial M}{\partial \delta_2} & \cdots & \frac{\partial M}{\partial \delta_n} \\ \frac{\partial N}{\partial \delta_1} & \frac{\partial N}{\partial \delta_2} & \cdots & \frac{\partial N}{\partial \delta_n} \end{bmatrix} \quad (8)$$

The following mixed optimization problem can be posed, which solves the error minimization problem and, if sufficient control authority exists, minimizes the difference between the control effector positions and a preferred set of effector positions (control minimization problem):

$$\min_{\delta} \left(\|\mathbf{B}\delta - \mathbf{d}_{des}\|_1 + \lambda \|\mathbf{W}_{\delta}(\delta - \delta_p)\|_1 \right) \quad (9)$$

subject to

$$\overline{\delta} \leq \delta \leq \underline{\delta} \quad (10)$$

where $\underline{\delta}$, $\overline{\delta}$ are the most restrictive lower and upper limits on the control effectors, respectively, and the 1-norm is selected so that linear programming techniques can be used to solve the problem.[3] In Equation 9, the parameter λ is used to weight the error and control minimization problems. For this work, it was determined that $\lambda = 0.01$ provided good error minimization while still driving the control effectors to the preferred values when sufficient control authority existed. The most restrictive lower and upper limits on the control effectors are specified as

$$\begin{aligned} \overline{\delta} &= \min(\delta_U, \delta + \dot{\delta}_{max}\Delta t) \\ \underline{\delta} &= \max(\delta_L, \delta - \dot{\delta}_{max}\Delta t) \end{aligned} \quad (11)$$

where δ_L, δ_U are the lower and upper position limits, δ is the last control effector command from the control allocation algorithm,

$\dot{\boldsymbol{\delta}}_{max}$ is a vector of rate limits, and Δt is the timestep or control update rate.

The vector $\boldsymbol{\delta}_p$ in Equation 9 is a preference vector. When sufficient control authority exists to drive the norm of acceleration errors to a sufficiently small value, the allocation algorithm will attempt to minimize the difference between the actual control deflections and $\boldsymbol{\delta}_p$. The preference vector is taken to be the pseudo-inverse solution so that

$$\boldsymbol{\delta}_p = -\mathbf{c} + \mathbf{W}^{-1}\mathbf{B}^T(\mathbf{B}\mathbf{W}^{-1}\mathbf{B}^T)^{-1}[\mathbf{d}_{des} + \mathbf{B}\mathbf{c}] \tag{12}$$

where $\mathbf{c}$ is an offset vector and $\mathbf{W}$ is a diagonal weighting matrix of the form

$$\mathbf{W} = \text{diag}[W_{\delta_{RF}}\, W_{\delta_{LF}}\, W_{\delta_{RR}}\, W_{\delta_{LR}}\, W_{\delta_{SB}}\, W_{\delta_{BF}}] \tag{13}$$

The elements of the offset vector $\mathbf{c}$ are all zero except for the elements corresponding to locked control surfaces. If a control effector is locked, then the corresponding entry in $\mathbf{c}$ is set to the negative of the locked location. Also, $\mathbf{W}_\delta$ in Equation 9 is a matrix used to weight the importance of driving each control effector to its preferred value. Using this preference vector allows one to analytically represent the control allocator in a robustness analysis of this system that is valid as long as no single axis is saturated and the commanded accelerations are feasible.

One last point to consider in the control allocation paradigm is the potential for slope reversals in the individual moment-effector relationships on this vehicle. Typically, slope reversals exist near the maximum or minimum values of control surface deflection. This can create problems when the actuator moves into non-monotonic regions of the moment-deflection curves, where it is possible for the effector to be limited to an unnecessarily restrictive range of positions. This phenomenon is a direct result of the use of a linear control allocator. Fortunately, this situation can be eliminated by ensuring that the moment curve is monotonic throughout the control space, which can be accomplished by pre-processing the aerodynamic data. In this way, the problems encountered with slope reversals are eliminated.

5 EXPLICIT MODEL FOLLOWING

The inner-loop flight control system for the X-40A was designed so that the closed-inner-loop system would exhibit a decoupled first order response to body-axis angular rate commands. An explicit model following scheme was used to shape the closed-inner-loop response and to compensate for modelling errors in the dynamic inversion control law. The desired roll, pitch, and yaw dynamics are described by:

$$\frac{\omega_m(s)}{\omega_{cmd}(s)} = \frac{K_{bw}}{s + K_{bw}} \tag{14}$$

where ω_m denotes either the desired roll, pitch, or yaw rate response of the explicit model and ω_{cmd} denotes the angular velocity command from the guidance and control interface. The term K_{bw} defines the nominal bandwidth of the desired dynamics. The system is designed to provide perfect tracking of the reference model when the dynamic inversion is perfect. Since this is never the case in practice, error compensation elements are used to mitigate the effects of inversion error. If the inversion is perfect, then the controlled element from the point of view of the explicit model following structure is a simple integrator. From block diagram algebra (see Figure 1), one can see that if the controlled element is a simple integrator, that is, if $\omega(s) = \frac{1}{s}\dot{\omega}_{des}(s)$, the $\omega(s)/\omega_m(s)$ transfer function is given by:

$$\frac{\omega(s)}{\omega_m(s)} = \frac{(K_D + K_{FF})s^2 + K_P s + K_I}{(K_D + 1)\, s^2 + K_P s + K_I} \tag{15}$$

which, when $K_{FF} = 1$, results in a double stable pole-zero cancellation with appropri-

Roll	Pitch	Yaw
$K_{bw_p} = 5$	$K_{bw_q} = 3$	$K_{bw_r} = 5$
$K_{P_p} = 7$	$K_{P_q} = 10$	$K_{P_r} = 7$
$K_{I_p} = 20$	$K_{I_q} = 10$	$K_{I_r} = 20$
$K_{D_p} = .1$	$K_{D_q} = .1$	$K_{D_r} = .1$
$K_{FF_p} = 1$	$K_{FF_q} = 1$	$K_{FF_r} = 1$

Table 1: Control system parameters for explicit model following control system.

ate choices of K_P, K_I, and K_D. Then, it is easily seen that

$$\frac{\omega(s)}{\omega_{cmd}(s)} = \frac{K_{bw}}{s + K_{bw}} \tag{16}$$

and perfect model following is achieved.

When the inversion is not perfect, the PID network attempts to drive the reference model tracking error to zero. Table 1 shows the gains for each channel of the explicit model following system. These gains were selected to provide acceptable tracking performance for pulse train commands in all channels.

5.1 INTEGRATOR ANTI-WINDUP AND REFERENCE MODEL BANDWIDTH ATTENUATION

When all control power has been exhausted in one or more axes, axis saturation has occurred. Control effector saturation results when one or more control surfaces is moving at its rate limit or lies on a position limit. In this case, control effector saturation is a necessary, but not sufficient, condition for the occurrence of axis saturation. Axis saturation can be detected through an analysis of the control allocation inputs and outputs. If $\mathbf{B}\boldsymbol{\delta} - \mathbf{d}_{des} \neq \mathbf{0}$ then axis saturation has occurred.

When an axis is saturated, all control authority has been expended and tracking errors can grow large. In order to prevent the integrator in the explicit model following prefilter from attempting to cancel tracking errors caused by axis saturation, an integrator anti-windup law is used to reduce the magnitude of the input to the integrator. The integrator anti-windup vector used in this design is given by:

$$\mathbf{I}_{aw} = \mathbf{K}_{AW}(\mathbf{B}\boldsymbol{\delta} - \mathbf{d}_{des}) \tag{17}$$

where $\mathbf{K}_{AW}$ is a gain. The integrator antiwindup compensation scheme operates on the difference between the output of the control allocator's internal model of the acceleration-deflection relationship, $\mathbf{B}\boldsymbol{\delta}$, and the desired control effector induced accelerations, $\mathbf{d}_{des}$. If no axes are saturated, then $\mathbf{B}\boldsymbol{\delta} - \mathbf{d}_{des} = \mathbf{0}$ and the control system operates normally. When $\mathbf{B}\boldsymbol{\delta} - \mathbf{d}_{des} \neq \mathbf{0}$, at least one axis is saturated and the state of the prefilter integrator is reduced by the anti-windup signal.

When an axis saturates, that is, when at least one component of $\mathbf{B}\boldsymbol{\delta} - \mathbf{d}_{des} \neq \mathbf{0}$, the inner-loop control system becomes degraded and most likely will not be able to track the nominal commands. One way of conveying this information to an outer-loop guidance command system is by way of inner-loop bandwidth. Nominally, the inner-loop bandwidth is set to K_{bw}, however, when axis saturation occurs, this bandwidth is reduced to avoid overdriving the actuators. The law used to reduce the inner-loop bandwidth is as follows: for all three axes, the input to the reduction law is $|\mathbf{B}\boldsymbol{\delta} - \mathbf{d}_{des}|$ and this is passed through a saturation block which, for the roll channel, is defined as

$$P_{sat} = \begin{cases} 0 \ if \ \ |\mathbf{B}\boldsymbol{\delta} - \mathbf{d}_{des}|_P < 0 \\ |\mathbf{B}\boldsymbol{\delta} - \mathbf{d}_{des}|_P \ \ if \ \ 0 \leq |\mathbf{B}\boldsymbol{\delta} - \mathbf{d}_{des}|_P \leq 1 \\ 1 \ if \ \ |\mathbf{B}\boldsymbol{\delta} - \mathbf{d}_{des}|_P > 1 \end{cases} \tag{18}$$

Similar definitions are also made for the pitch and yaw channels. Now, the modified

or new bandwidths $(K_{bw_P}, K_{bw_Q}, K_{bw_R})$ are defined by

$$\begin{aligned} K_{bw_P} &= \left(\tfrac{-9}{10} P_{sat} + 1\right) K_{bw_{Pnom}} \\ K_{bw_Q} &= \left(\tfrac{-5}{6} Q_{sat} + 1\right) K_{bw_{Qnom}} \\ K_{bw_R} &= \left(\tfrac{-9}{10} R_{sat} + 1\right) K_{bw_{Rnom}} \end{aligned} \tag{19}$$

where $K_{bw_{Pnom}}, K_{bw_{Qnom}}, K_{bw_{Rnom}}$ are the nominal bandwidths which were set to 5, 3, 5 $\frac{rad}{sec}$, respectively. Thus, the range of bandwidth for the roll and yaw channels is 0.5 to 5 $\frac{rad}{sec}$ and 0.5 to 3 $\frac{rad}{sec}$ for the pitch channel. Figure 1 shows the complete inner-loop block diagram while Figure 2 reveals the bandwidth modification logic. Displayed in Figure 1 are the prefilters, dynamic inversion, control allocation, and the integrator antiwindup scheme. For implementation in a digital simulation, all continuous time blocks were converted to equivalent discrete time blocks using a Tustin transformation.

6 IN-FLIGHT SIMULATION RESULTS

The complete integrated control system, consisting of a reconfigurable inner-loop control law, guidance gain adaptation controller, and trajectory reshaping algorithm were tested on a simulated X-40A. The Total In-Flight Simulator (TIFS) research aircraft was used to "mimic" the X-40A as closely as possible. In this section, results from the flight tests will be presented for two specific failure cases.

Under ideal circumstances, the transfer function for each channel of the inner-loop can be represented by a first-order lag as shown in Equation 14. For the roll and yaw channels, $K_{bw} = 5\frac{rad}{sec}$ while for the pitch channel, $K_{bw} = 3\frac{rad}{sec}$. Some of the data available from the flight tests are time histories of roll, pitch, and yaw rate commands to the inner-loop and the actual roll, pitch, and yaw rates produced as outputs of the inner-loop. In order to ensure that the inner-loop is working properly, the roll, pitch, and yaw rate commands were filtered by an ideal version of the inner-loop, namely, $\frac{5}{s+5}$ for the roll and yaw channels and $\frac{3}{s+3}$ for the pitch channel. If the inner-loop is working properly, then these ideal responses should be nearly equivalent to the actual roll, pitch, and yaw rate responses. Plots of this nature are shown for representative failure cases. Also, the bandwidth of each inner-loop channel will be displayed.

The first failure case considered was the bodyflap stuck at 5°. This failure causes a pitching moment to be applied to the vehicle, which the remaining control effectors must counteract. Figure 3 shows the ideal and actual roll, pitch, and yaw rates for this case while Figure 4 displays the bandwidths for each channel. Clearly, the inner-loop is working as expected as the body-axis rate commands filtered by ideal first-order lags (traces labelled ideal) are nearly equivalent to the body-axis rates produced by the flight test vehicle (traces labelled actual). In this case, none of the three axes became saturated as all three bandwidths remain at their original value for the duration of the flight.

In the second failure case, the right and left ruddervators are locked at 0°. For the X-40A, the ruddervators are by far the most effective aerodynamic control surfaces, and thus, this type of failure will require large amounts of control deflections from the remaining weaker control surfaces to compensate for the loss of control power. Figure 5 shows the ideal and actual body-axis rates while Figure 6 displays the bandwidth for each axis. Once again, the inner-loop is operating as expected: the ideal body-axis responses are equal to the actual body-axis responses. Hence, the inner-loop, from an input/output perspective, looks like a first-order transfer function. In terms of axis saturation, it appears that the roll and pitch

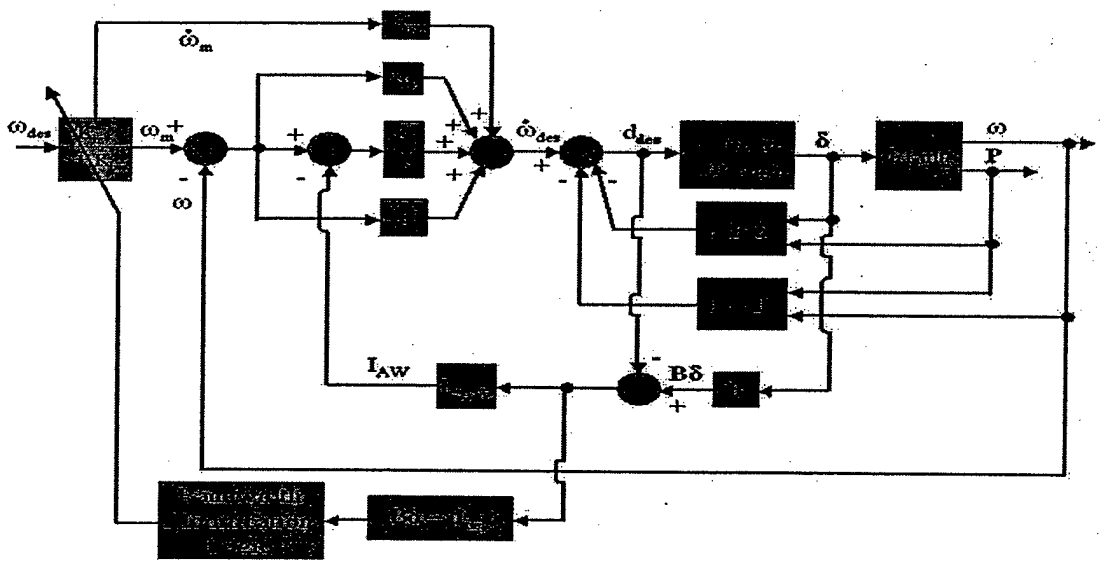

Figure 1: Inner-Loop Block Diagram.

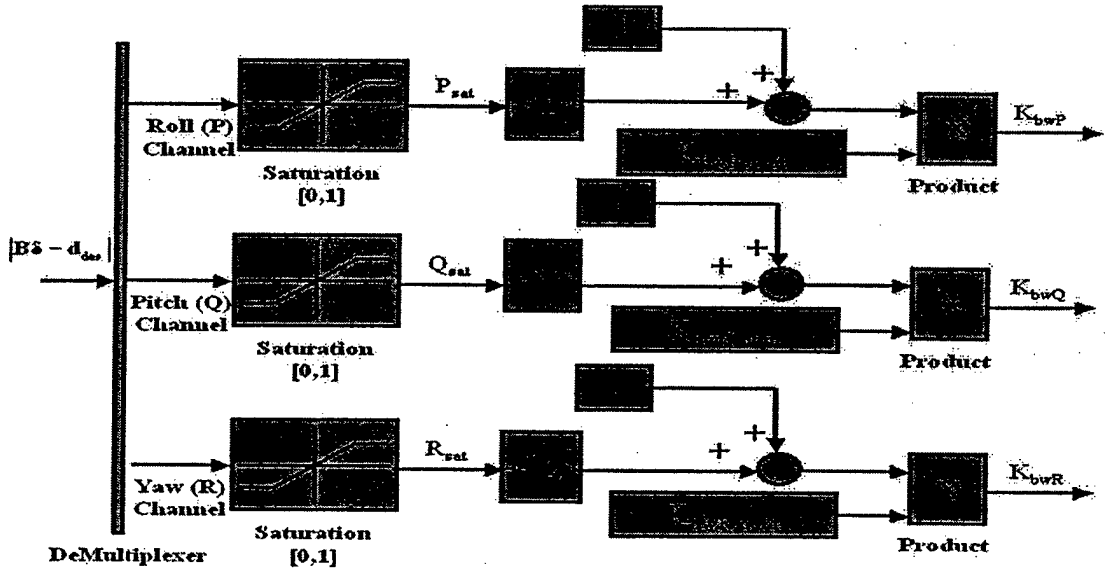

Figure 2: Bandwidth Modification Logic.

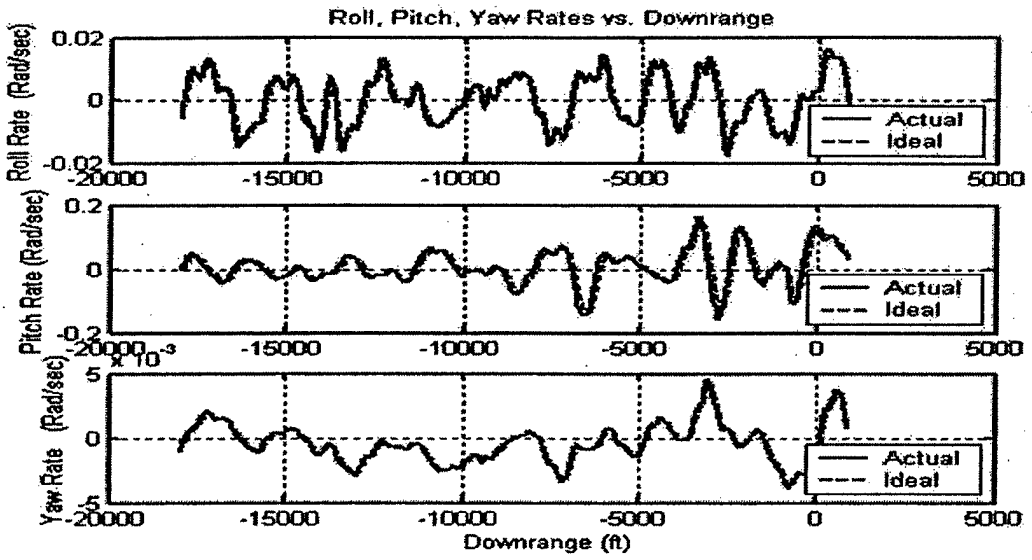

Figure 3: Roll, Pitch, and Yaw Rates vs. Downrange, Bodyflap = 5°.

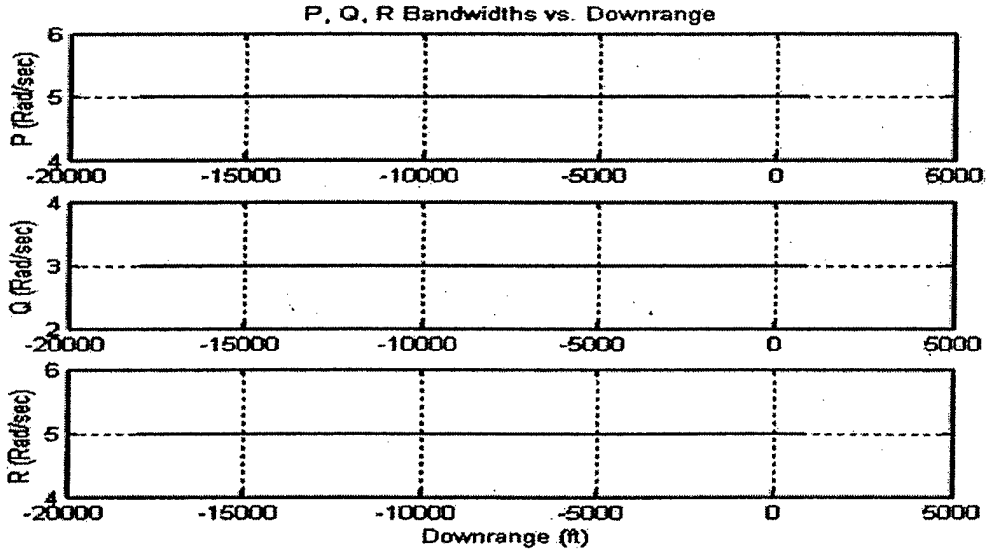

Figure 4: Bandwidths vs. Downrange, Bodyflap = 5°.

axes are rarely saturated, however, the yaw axis is saturated regularly. The problem here lies in the fact that since both ruddervators have failed, the flaperons are responsible for both roll and yaw control (the bodyflap and speedbrake essentially produce only pitching moments). These two surfaces alone cannot simultaneously produce the required roll and yaw and hence, the flaperons become rate limited. When rate limiting occurs, the yaw axis component of $\mathbf{B}\boldsymbol{\delta} - \mathbf{d}_{\mathbf{des}} \neq \mathbf{0}$, the bandwidth modification logic reduces the bandwidth of the yaw channel, and this information is passed to the guidance loops. The guidance loops, in turn, modify their gains when the inner-loop becomes degraded so as to reduce the demands on the inner-loop and maintain stability.

7 CONCLUSIONS

In this work, an inner-loop control law was designed for a modified version of the X-40A Reusable Launch Vehicle. The control law utilized a dynamic inversion controller and a linear programming based control allocation algorithm. To shape the closed-loop dynamic response, an explicit model following prefilter was designed. Nominally, the inner-loop was designed to display a first-order lag type response. However, in the presence of axis saturation, inner-loop bandwidth is decreased so that the demands on the actuators are reduced. A complete description of the guidance adaptation can be found in the companion paper.[7]

References

[1] "Application of Multivariable Control Theory to Aircraft Control Laws," Tech. Rep. WL-TR-96-3099, Wright Laboratory, WPAFB, OH, 1996.

[2] A. B. Page and M. L. Steinberg, "A Closed-loop Comparison of Control Allocation Methods," in *Proceedings of the 2000 Guidance, Navigation and Control Conference*, AIAA 2000-4538, August 2000.

[3] M. Bodson, "Evaluation of optimization methods for control allocation," *Journal of Guidance, Control and Dynamics*, vol. 25, no. 4, pp. 703–711, 2002.

[4] J. D. Schierman, J. R. Hull, and D. G. Ward, "Adaptive Guidance With Trajectory Reshaping For Reusable Launch Vehicles," in *Proceedings of the 2002 Guidance, Navigation and Control Conference*, AIAA 2002-4458, August 2002.

[5] B. Etkin, *Dynamics of Atmospheric Flight*. John Wiley & Sons, Inc., 1972.

[6] D. B. Doman and M. W. Oppenheimer, "Improving Control Allocation Accuracy for Nonlinear Aircraft Dynamics," in *Proceedings of the 2002 Guidance, Navigation and Control Conference*, AIAA 2002-4667, August 2002.

[7] J. D. Schierman, N. Gandhi, J. R. Hull, and D. G. Ward, "Flight Test Results Of An Adaptive Guidance System For Reusable Launch Vehicles," in *Proceedings of the 2004 Guidance, Navigation and Control Conference*, AIAA 2004-xxxx, August 2004.

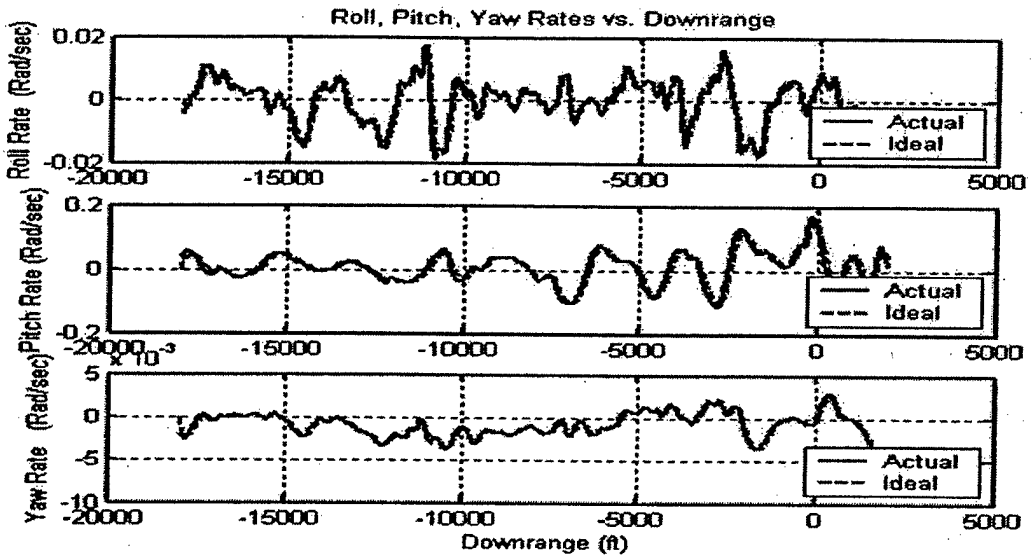

Figure 5: Roll, Pitch, and Yaw Rates vs. Downrange, Right Rudder = Left Rudder = 0°.

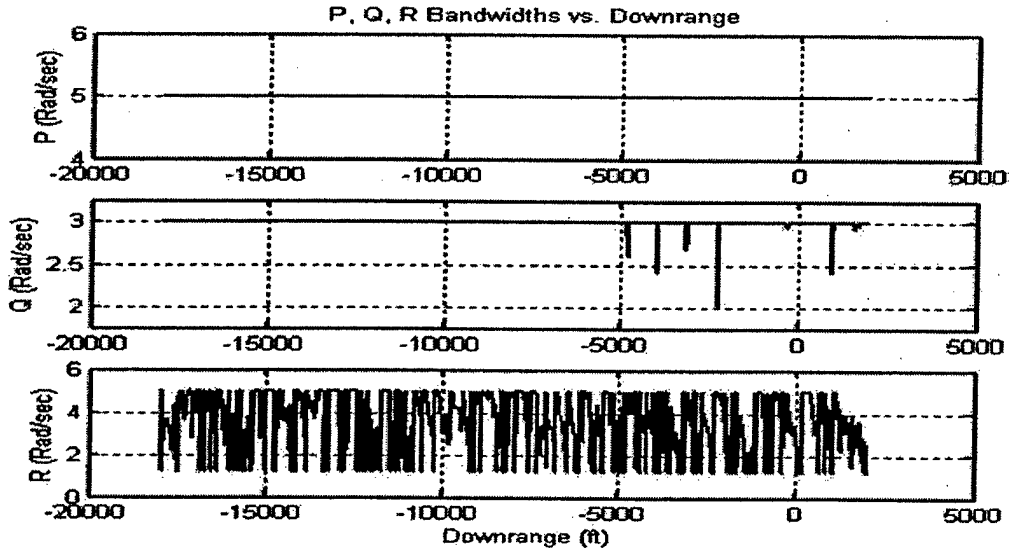

Figure 6: Bandwidths vs. Downrange, Right Rudder = Left Rudder = 0°.